A comparative study of the performance of IR detectors vs. high-speed cameras under dynamic loading conditions

G.G. Goviazin[1,2], A. Shirizly[1,2], D. Rittel[1]

[1] Faculty of Mechanical Engineering, Technion – Israel Institute of Technology, 32000 Haifa, Israel.

[2] Rafael, POB 2250 (774), Haifa 3102102, Israel.

- Corresponding author: G.G. Goviazin – gil.goviazin@gmail.com

Abstract

Background The conversion of plastic work to heat and its efficiency (the Taylor-Quinney coefficient - TQC), are traditionally measured using infrared single-detectors (named detectors from here on) which measure the temperature at a single point on the surface. Lately, fast infrared cameras (focal plane array of detectors that measures a 2-dimensional field of view on the surface) have been increasingly used for that purpose too, but no systematic study has been carried out yet to compare the respective performance of each monitoring system for impact loading conditions. **Objective** A comparison between the two techniques (infrared detector and infrared fast camera) is reported for commercial 316L stainless steel under dynamic loading in the Kolsky bar. The respective merits and limitations of each setup are compared and discussed. **Methods** Cylindrical specimens were loaded at a strain rate of about 3000 [1/s] in a split Hopkinson pressure bar (Kolsky bar) apparatus. The transient temperature change was monitored in two separate series of experiments: In the first, we used a liquid N_2 cooled Mercury-Cadmium-Telluride (MCT) detector made by InfraRed Associates (USA) with a 1.5 MHz sampling rate, and in the second, a Telops FAST M2K high-speed infrared camera made by Telops (Canada) based on Indium Antimonide (InSb) array-detector and with a sampling rate of up to 90 kHz. **Results** Temperature changes under impact were successfully measured and compared using the two distinct techniques. In addition, the IR camera rendered a satisfactory thermal and visual recording of dynamic shear failure of various specimens. **Conclusions** The *integral* Taylor-Quinney coefficient (β_{int}) can be assessed using either infrared detector or fast infrared camera alike, under dynamic loading conditions. However,

the evaluation of the *differential* TQC (β_{diff}) necessitates high sampling rates such as those enabled by infrared single detectors as compared to infrared high-speed cameras.

Keywords

- Infrared detector, high-speed infrared camera, Taylor-Quinney coefficient, Thermomechanical coupling, Stored energy of cold work.

Introduction

Starting at least from the early days of Tresca [1], it is well-known that large amounts of heat can be generated in materials undergoing large plastic deformation at high strain rates. Under adiabatic conditions, the heat causes a significant temperature rise, which may in turn affect the mechanical response of the impacted material, as reflected in constitutive models such as the popular Johnson-Cook model [2].

Early work by Taylor and Quinney [3] (discussed later) examined the ratio of thermal to mechanical work under transient conditions, also known as the Taylor-Quinney coefficient, TQC [3]. With the advent of infrared detectors, the TQC has been measured for various materials under various loading conditions, such as tension, compression, shear, and mixed modes [4–11]. While this paper is not meant to review the various results available of the TQC, a central issue is that of the simultaneous measurement of the stress, strain, and temperature of the loaded specimen. More specifically, since the measurements of dynamic loads and displacements are almost "routine" procedures using the Kolsky apparatus [12, 13], the remaining issue is that of *real-time temperature measurement*.

At this stage, it must be clarified that, whereas the TQC is a central point of this paper, temperature measurements are also necessary for other assessments such as the evolution of the mechanical properties with the occurrence of dynamic shear localization [14], the occurrence of hot spots and their relevance for granular mechanics [15], and of course metal machining [16], just to name a few. Different techniques have been used for temperature measurements over the years, such as calorimetry [3, 17], thermocouples [18–20], infrared (IR) detectors [5–8, 21, 22] and more recently IR cameras [23–27]. Although Taylor and Quinney, in one of the first works regarding the conversion of plastic work to heat, used a calorimeter [3], it seems that IR detectors have long dominated the field of transient dynamic temperature measurements [11, 28–35]. Recent technological progress yielded fast IR cameras which were

used to evaluate the specimen's surface temperature change, and thus the (integral) TQC for some materials [24, 36], and in some cases, the differential TQC, was evaluated [37].

IR detectors have a much higher sampling rate (on the order of 1.5 MHz) as compared to the fast IR cameras (on the order of 100 kHz). In other words, thermal cameras "under-sample" the signal that would be acquired with a detector. This said, it seems that no comparative study has yet been made between IR detectors and fast IR cameras. Such a comparative study is the purpose of this paper.

The paper is organized as follows: First, some elements of the basic theory are presented regarding IR measurements and the parameters for comparison between both techniques are discussed. Experimental procedures, methods, materials, and equipment are discussed next. Temperature measurements and typical failure patterns are reported next, followed by a discussion comparing the relative performance of each measurement technique.

Theory

β_{int} and β_{diff} evaluation

A well-known Taylor-Quinney relation expresses the conversion of plastic work into heat [3, 4]:

$$\beta_{int} = Q/W_p \qquad (1)$$

when β_{int} expresses the amount of plastic work converted into heat and is named the Taylor-Quinney coefficient (TQC), Q is the amount of heat released, and W_p is the plastic work. The released heat Q is calculated by:

$$Q = \rho C_p \Delta T \qquad (2)$$

when ρ is the materials density, C_p is the specific heat at constant pressure, and $\Delta T = T - T_{initial}$ is the temperature rise in the specimen [4]. The plastic work is defined by:

$$W_p = \int_0^{\varepsilon_p} \sigma_{ij} d\varepsilon_{ij}^p \qquad (3)$$

The *integral* TQC [4]can thus be written as:

$$\beta_{int} = \frac{\rho C_p \Delta T}{\int_0^{\varepsilon_p} \sigma_{ij} d\varepsilon_{ij}^p} \qquad (4)$$

In Taylor and Quinney's work with copper under dynamic loading from 1934 [3], a TQC value of $\beta_{int} = 0.9$ was reported, that has been widely used since [14, 38]. Note that in many cases, this value is used without taking into consideration properties like material (crystal structure, heat treatment conditions, etc.) and loading regime changes (tension, compression, shear,

mixed loading, etc.). Although in some cases a TQC of $\beta_{int} = 0.9$ is justified, it has been shown in many cases that TQC can be anywhere in the range of $0.2 - 0.9$ for different materials, and even for the same material under different loading conditions [7, 29, 30, 36, 37, 39]. All these indicate that not only the mechanical properties should be tested under working regime strain rate and tractions, but also the temperature of the part (specimen) should be monitored especially under dynamic loading where thermal conditions are close to adiabatic due to lack of time for conduction.

The first law of thermodynamics (conservation of energy) yields the following coupled heat equation [40]:

$$\kappa\nabla^2 T - \alpha(3\lambda + 2\mu)T_0\dot{\varepsilon}^e_{kk} + \beta_{diff}\sigma_{ij}\dot{\varepsilon}^p_{ij} = \rho C_p\dot{T} \qquad (5)$$

Where κ stands for the heat conductance and α is the thermal expansion coefficient. λ, μ are the Lamé constants, T_0 is the initial temperature and $\dot{\varepsilon}^e_{kk}$ is the trace of the elastic strain rate tensor. In this equation, β_{diff} represents the *instantaneous* fraction of plastic work converted to heat [4]. Under high strain and strain rate loading, adiabatic conditions are prevailed, and the elastic term is neglected which yields:

$$\beta_{diff}\sigma_{ij}\dot{\varepsilon}^p_{ij} = \rho C_p\dot{T} \qquad (6)$$

It is noted that β_{diff} is part of the coupled heat equation (eqn. 5) whereas β_{int} basically evaluates the average efficiency of the thermomechanical conversion up to a given strain. However, β_{diff} is seldom reported, which might be due to the necessity of evaluating the incremental temperature at a high sampling rate, characteristic of IR detectors.

IR detectors' and cameras' principle for temperature measurement

Infrared (IR) wavelength has a large bandwidth starting from around 0.75 μm up to about 14 μm. Different types of infrared detectors made of a verity of materials (e.g., MCT and InSb as in this work) available for covering part of that large bandwidth. The detector itself can be a photodiode or a phototransistor, which changes its resistance and voltage according to the IR light received (in the specific working range of wavelengths a particular detector works in). For the simplicity of further explanation let's suppose we have some thermal emission (as expressed by the Stefan-Boltzmann's Law [41]) and this emission is projected on an area equivalent to the one covered by a IR sensing device, e.g., IR detector or fast IR camera:

$$P = A\sigma\varepsilon(T^4 - T_0^4) \qquad (7)$$

Where P stands for the net power radiated, A is the body surface area, σ is the Stephan-Boltzmann constant, ε stands for emissivity, T is the measured temperature and T_0 is the

reference temperature. The body surface (A) is usually limited to the detector's area (the sensing device in an IR camera is a detector too), and to expand the measured area some optics is used as in the IR camera case. In order to have better resolution, a larger array of detectors is needed [34]. The emissivity (ε) depends strongly on the material being measured and its surface conditions [41]. The detector takes this change into account by a former calibration of the radiometric output, performed on an opportune calibrating sample. For the camera, unless the exact emissivity is known or can be found, it is advised to try and turn the examined object to a black body ($\varepsilon = 1$) by e.g., painting the body in very thin black opaque (i.e., matt) color and hence eliminate/reduce this dependency as proposed in the user manual of the thermal camera by Telops (the manufacturer of the camera) [42]. On the other hand, a calibration can be performed [26, 36] for the camera too, but it increases the additional effort of the experiment. There are two main types of IR detectors (also used in IR cameras), when those used in this work are the Mercury - Cadmium - Telluride (HgCdTe or also known as MCT for the detector) and the Indium – Antimonide (InSb) for the camera. IR emission detection by sensors is sensitive to environmental thermal changes, i.e., every environmental thermal fluctuation and sometimes even the kind of light (worm bulbs with warm light as opposed to LED) change will affect the measured temperature value especially when the temperatures of the object and the environment are close. For this reason, it is important to conduct a series of repetitive tests and to guarantee that the measured data is reliable [43].

Relying on the work done by Rabin and Rittel [44], one can assume homogenous temperature inside and on the surface of a given *metallic specimen under dynamic loading*. Hence the thermomechanical coupling, i.e. the amount of energy converted to heat from plastic deformation in a given specimen, is represented correctly although the measurements are done on the surface of a specimen rather than in its core. The above is true for any surface temperature sampling technique.

Materials and Methods

Materials and specimens

In this work, three materials were tested: 316L stainless steel (SS316L) in the as received condition, commercially pure annealed Titanium grade 4 (CP Ti) and annealed Titanium grade 5 (Ti6Al4V). The main comparative study between the infrared (IR) detector and IR fast camera was done only on the SS316L. Both the CP Ti and the Ti6Al4V were used to investigate

additional topics with the IR fast camera, such as localized shear and failure in the localized shear plane and not for comparative study, although some comparison to literature is presented. All specimens were painted in matt-black paint (using a thin layer like a marker but not spray to avoid IR emission blocking) to have a closer representation to a black body as discussed before. The comparative study on SS316L and the study of temperature rise during failure along a shear localization plane in Ti6Al4V, were carried on cylindrical specimens, having different diameters as presented in Figure 1. Temperature rise due to localized shear and/or fracture was examined using shear compression specimens with 45˚ groove (SCS-45) [45, 46] whose dimensions are presented in Figure 2.

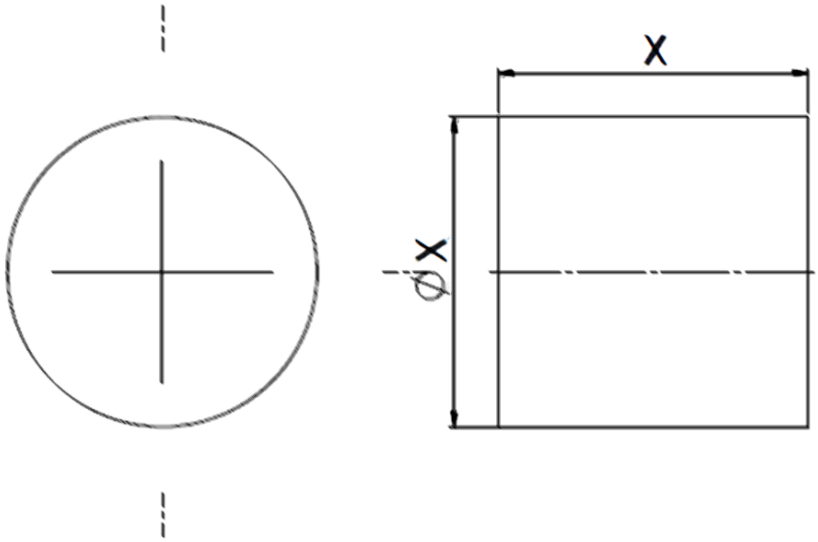

Material	SS316L	Ti6Al4V
X [mm]	7	6

Figure 1: Cylindrical specimens used for SS316L and Ti6Al4V tests.

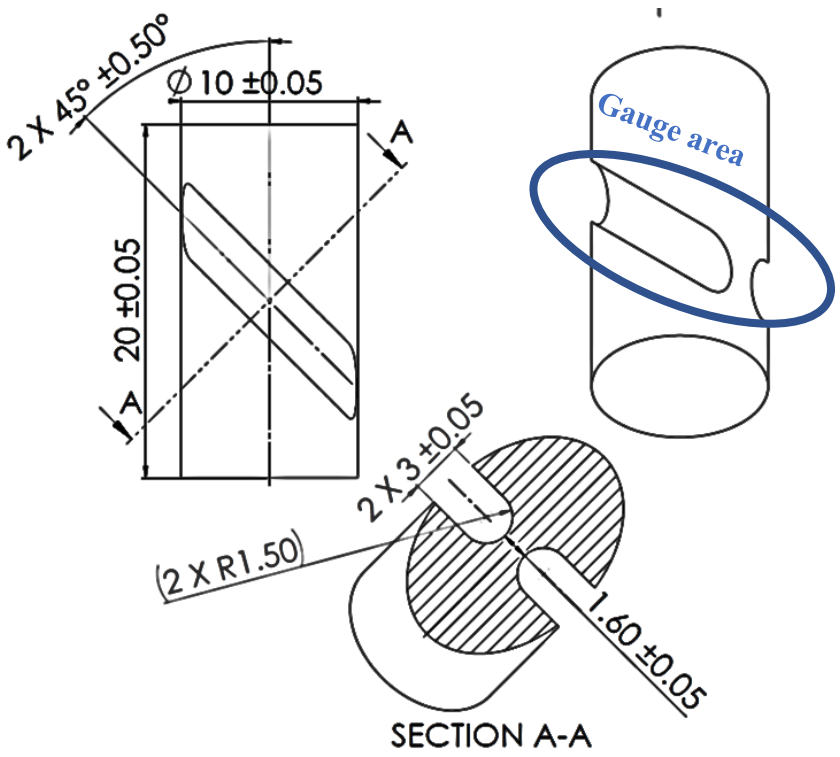

Figure 2: SCS specimen used for CP Ti tests.

Split Hopkinson Pressure Bar (Kolsky bar) apparatus

All tests were carried out using a split Hopkinson pressure bar (SHPB) apparatus [12, 13] with 19.05mm diameter, made of C300 steel Maraging. The incident and transmitted bars are 2 and 1 meters long, respectively. A 250 mm long striker made of the same material and bars' diameter was used to yield a strain rate of about 3000 1/s for about 100 µs. A homemade Wheatstone bridge for strain gauges measurements and as a trigger setup for the IR fast camera were used, and a Nicolet 440 oscilloscope was used for data acquisition.

Infrared Detector

An InSb / HgCdTe 2-color detector (InfraRed Associates, USA) was used. This specific setup contains two detectors, an InSb detector for 1-5.5 µm wavelength and a HgCdTe detector for 5.5-12.55 µm wavelength. The InSb is suitable for higher temperatures while the HgCdTe is for lower, so that for the present experiment we used only the HgCdTe detector. The detector operates at 77 K and hence its Dewar was filled with liquid nitrogen. The detector's amplifier for the 1.5 MHz sampling rate was connected to a Nicolet 440 oscilloscope for data acquisition. The full calibration routine is discussed elsewhere [43] hence the procedure will only be discussed briefly in this paper. Since the detector in use has no built-in calibration unit that converts the detector's output voltage to temperature, a calibration procedure is needed. The

first step of the calibration consists of heating up a dummy specimen from the tested material which is monitored by both a thermocouple and the IR detector. After the specimen has been heated up to a steady temperature, the soldering iron is turned off and the specimen is left for cooling. The cooling period of the specimen, which takes a long time without rapid changes in temperature, is simultaneously monitored by both the thermocouple and the detector and recorded using a data acquisition system (oscilloscope in this case). The recorded data enables one to correlate the thermocouple and detector's output voltages. One can thus construct a calibration curve which transforms the detector's output voltage into temperature during a dynamic experiment without the need in thermocouples.

Fast Infrared Camera

Fast full-field infrared imaging was achieved using our Telops (Canada) FAST M2k infrared camera, which provides a frame rate of up to 90,000 frames per second (FPS) with 64X4 pixels resolution, namely a frame each 11.1 μs. In this study 69,000 (each 14.5 μs) and 57,000 (each 17.5 μs) FPS were used with 64X12 and 64X20 pixels resolution, respectively. The trade-off of using higher resolution is a wider view field which might capture more information while reducing the frame rate (not reaching the maximum of 90,000 FPS), this trade-off fitted the materials' behavior during the experiments done in this work. In the specific camera used in this work, the working distance at which a sharp picture is achieved is 1 meter, indicating that each pixel is 0.55X0.55 mm. The focus of a picture is crucial for correct thermal measurements. Another important parameter for calibration is the integration time, which was set after some testing to 4μs to allow for high-speed imaging on the one hand and prevent pixels' saturation on the other hand. The camera was triggered by the Hopkinson bar's strain gauges and was controlled via the dedicated program developed by Telops. The camera comes with built in calibration files and four built in filters, each filter for a specific range of temperatures.

- It was decided to have the tests done under direct line of sight, although materials passing IR emission could be used for shielding the camera from flying specimens. Common shield materials are not homogeneously transparent in the IR spectrum ranges and therefore strongly influence the acquired thermograms as presented in Figure 3, hence weren't used here. In addition, and as was explained above, since the camera assumes black-body emissivity ($\varepsilon = 1$) for its temperature output, each specimen was brought closer to black-body by painting in black according to the manufacturer's recommendation.

The temperature used for the camera's measurements analysis with cylindrical specimens was calculated as the mean value of all pixels along the center plane of the specimen, as presented in Figure 4, as the most isolated place from end effects and inhomogeneities in strain. For the SCS the average temperature along the gauge was used, Figure 2 presents the gauge definition.

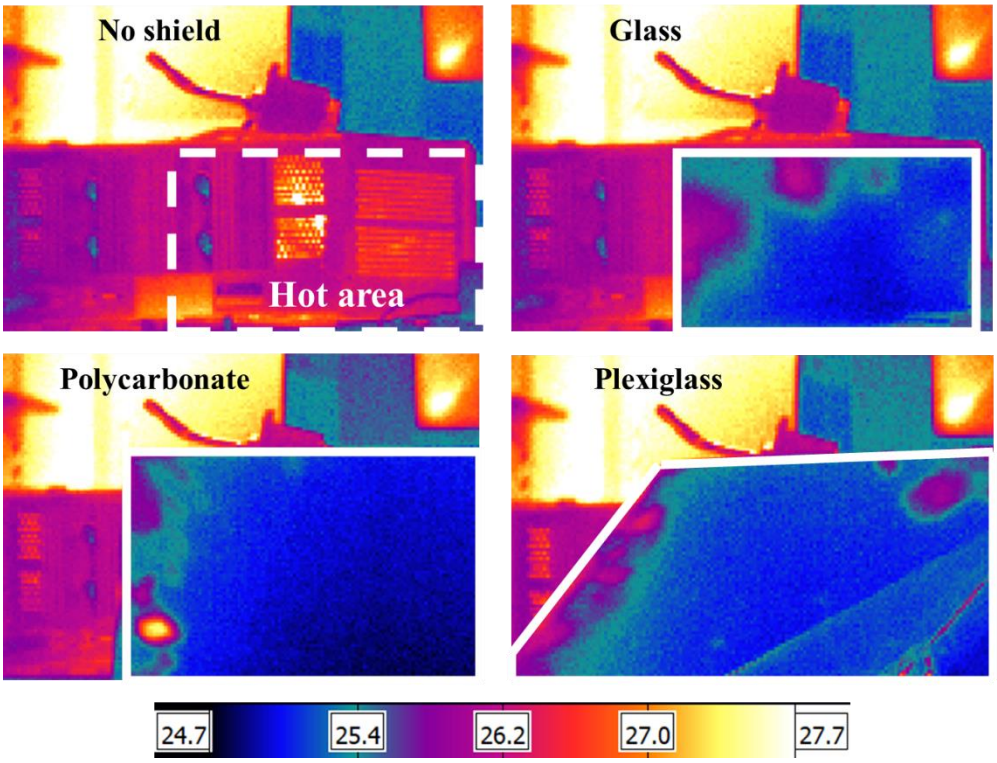

Figure 3: Different shields filter out the IR emission, and hence direct line of sight was used in this work. The shield materials are specified by name and white border for each picture.

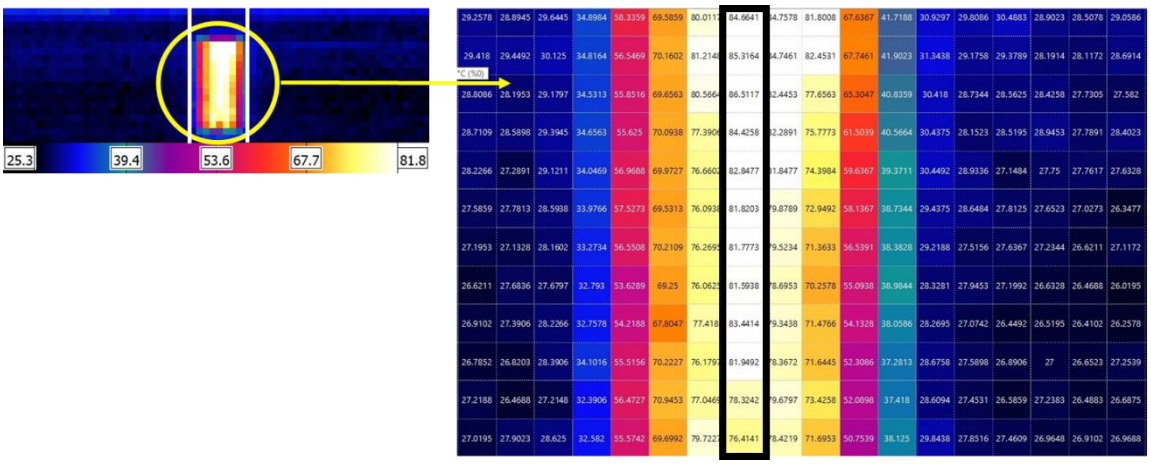

Figure 4: A close up on a specimen during testing. The SHPB's edges are marked with white lines. The middle column (center plane) at the center of the specimen, as marked in black box

in the enlarge frame, was used for mean temperature calculation in the specimen. The ability to access each pixel's temperature is shown too.

Results

Experimental results for 316L stainless steel (SS316L), Titanium grade 5 (Ti6Al4V), and commercially pure Titanium grade 4 (CP Ti) are presented. The SS316L was used for the comparative study between the IR detector and fast IR camera, Ti6Al4V was used for post failure characterization, and the CP Ti was used for localized shear characterization. The Taylor-Quinney coefficients, defined above, are among the central physical parameters of relevance to the thermo-mechanical description of materials. Both β_{int} and β_{diff} are derived from the temperature measurements and stress-strain relations, however it was decided to show only the basic measured variables (stress-strain relation and temperature) rather than the mathematically manipulated values, since we are comparing techniques and not materials in this work.

Comparative study – IR detector and fast IR camera on SS316L

Split Hopkinson pressure bar (SHPB) tests were carried out on a cylindrical specimen (7mm in diameter and length) in compression and under *ca.* 3000 1/s strain rate. A total of 5 specimens were tested with the IR detector, and additional 2 with the thermal camera, all possessing a good repeatability. The snapshots from the IR camera are presented in Figure 5. All signals were synchronized in time and a specific example of two tests is presented in Figure 6, one using the IR detector and the other using the camera. After time synchronization was done, each temperature could be related to a specific strain value. Using this correlation between the temperature and strain for each test and IR measurement methos and combining with the stress strain data achieved from SHPB experiments, one can build the material's characterization curves as presented in Figure 7. The mean value of the stress and temperature as a function of strain are presented with a full line, while the standard deviation is represented by the shaded area. A satisfactory comparison was achieved between the IR detector and IR fast camera readings, resulting in almost identical results.

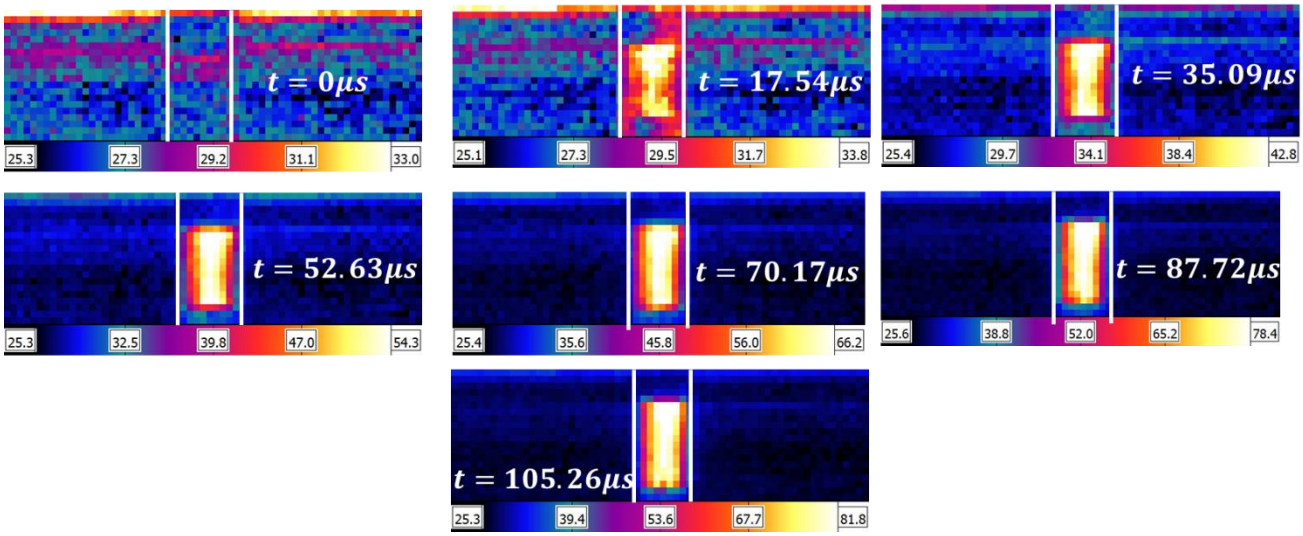

Figure 5: Snapshots of SS316L at 57,000 FPS with 64x20 pixels resolution. The SHPB's edges are marked with white lines and the time at each frame is written.

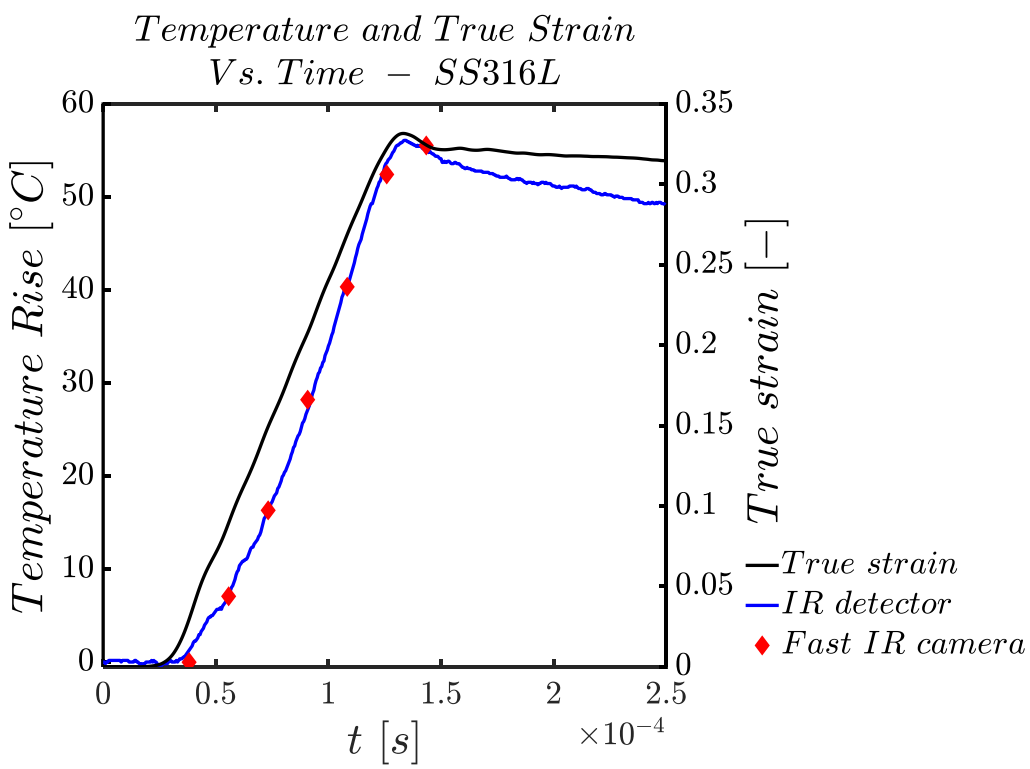

Figure 6: Temperature rise (ΔT) and true strain Vs. time for SS316L. Synchronization of the fast IR camera shows good correlation to the measured temperature using the IR detector.

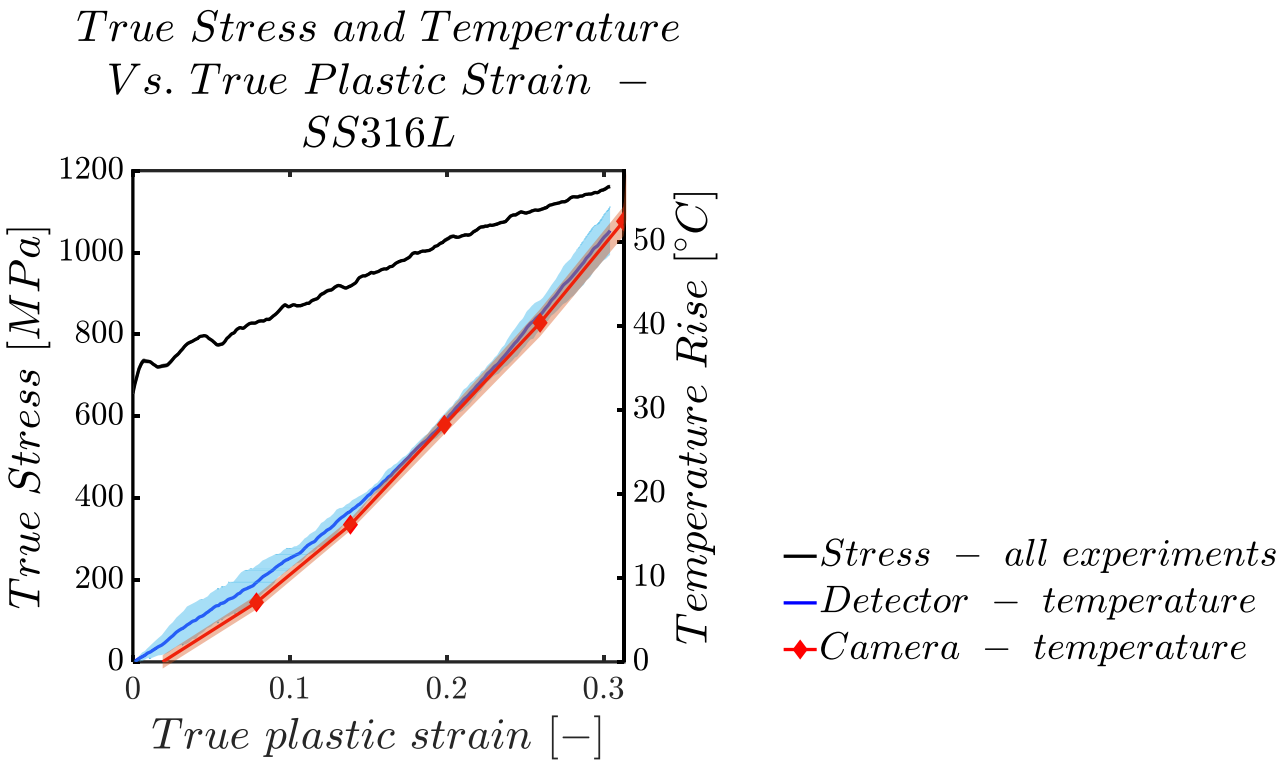

Figure 7: True stress and temperature rise (ΔT) Vs. true plastic strain for SS316L. The black line represents the stress-strain plot for all specimens tested. Blue and red lines represent the temperature rise with strain for the detector and camera, respectively. The shaded areas represent the standard deviation. The diamond markers represent the measured points with the camera.

Extending the sampling time - Failure along a shear plane measurement

After establishing the satisfactory correlation for temperature measurements between both IR techniques, it was decided to extend the framework and to investigate shear band failure with the fast IR camera. For that a Ti6Al4V was used due to its known failure mode along a shear plane. The clear advantage of the camera over the detector, i.e., full field visualization, was taken into advantage to examine the deformation and post failure temperatures. The snapshots are presented in Figure 8 and the stress – temperature – strain relation is plotted in Figure 10. Figure 8 shows the specimen being almost homogeneously heated up to some point ($t = 76.92\ \mu s$) where a localized shear plane can be seen, the specimen after test is shown in Figure 9. The high temperatures along the shear plane were above the saturation value of the first filter (having a temperature range of $-20 \div 168$ ℃), hence the test was repeated using the higher temperature range filter lens (having a temperature range of $129 \div 450$ ℃). Here, temperatures above 300 ℃ were recorded along the failure shear plane. Synchronizing signals in time as was done for the SS316L and extracting temperature and

strain relation enabled the construction of Figure 10. Using a detector limits the field of view due to its small area detected once the incident bar of the SHPB pushes the specimen away, but the camera on the other hand enables the analysis of longer timescales even after specimen has failed. Hence failure modes and temperatures can be studied using the camera. Comparing results for Ti6Al4V from literature, measured by an IR detector, reveals similar results up to failure [7]. As presented in Figure 10, the specimen is almost homogenously heated until failure, and only when final failure sets in (adiabatic shear band and friction) the recorded temperature increases at a much higher rate. This experiment emphasizes the wide range of applications for full material characterization, as mentioned in the introduction. The increasing dispersion of the measurement temperature presented in Figure 10 is due to the averaging of the central column of the specimen, as was shown in Figure 4 for SS316L. However, the localized hot shear plane as respect to the other part of the specimen introduce increasing temperature differences, and hence increasing deviations in temperature's mean value.

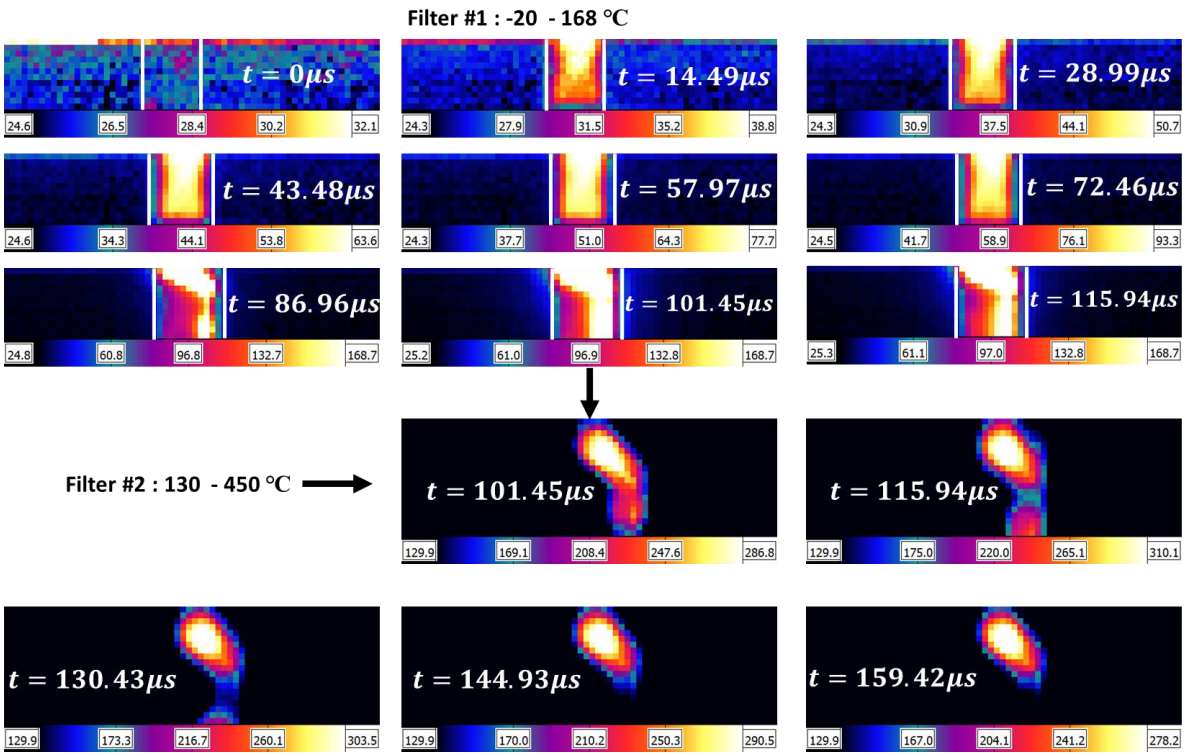

Figure 8: Snapshots of Ti6Al4V at 69,000 FPS with 64x12 pixels resolution. The SHPB's edges are marked with white lines and the time is written for each frame. At the post-failure step a failure along a shear plane can be seen ($t = 86.96\ \mu s$). A large temperature increase caused by the shear plane is presented from $t = 86.96\ \mu s$ with both filters (different temperature range).

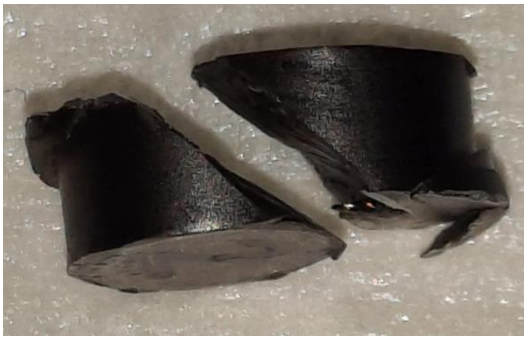

Figure 9: Ti6Al4V cylindrical specimen after test. The shear failed plane can be seen.

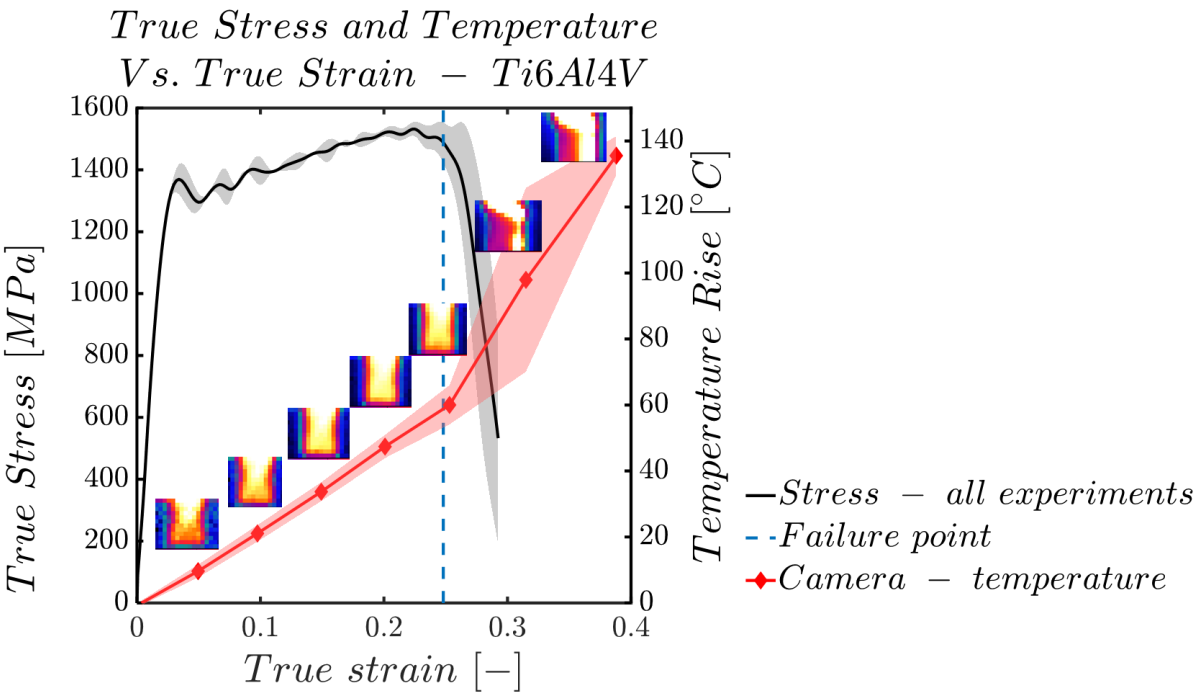

Figure 10: True stress and temperature rise (ΔT) Vs. true plastic strain for Ti6Al4V. The black line represents the stress-strain plot for all specimens tested, when the straight light blue line marks the failure point in the specimen. The red line represents the temperature rise with strain as measured by the camera. The diamond markers represent the measured points with the camera when the corresponding frame is attached. The shaded areas represent the standard deviation.

Examining the ability of local measurements along a shear plane

For completion, a shear compression specimen (SCS) made of CP Ti was tested with the same experimental configuration, and the experimental sequences are presented in Figure 11. Although the deformation is localized in a thin gauge compared to the large size of the pixels (0.55 X 0.55 mm), it was possible to see the expected and desired result. At the beginning a

moderate temperature rise is detected only along a well-defined plane, as reported earlier for shear specimens [7, 10, 11], of the gauge and up to failure. From that point, the temperature rises dramatically due to failure as was presented above for Ti6Al4V. Once again, the post-failure temperature rise is very high and hence the use of the higher temperature lens was needed.

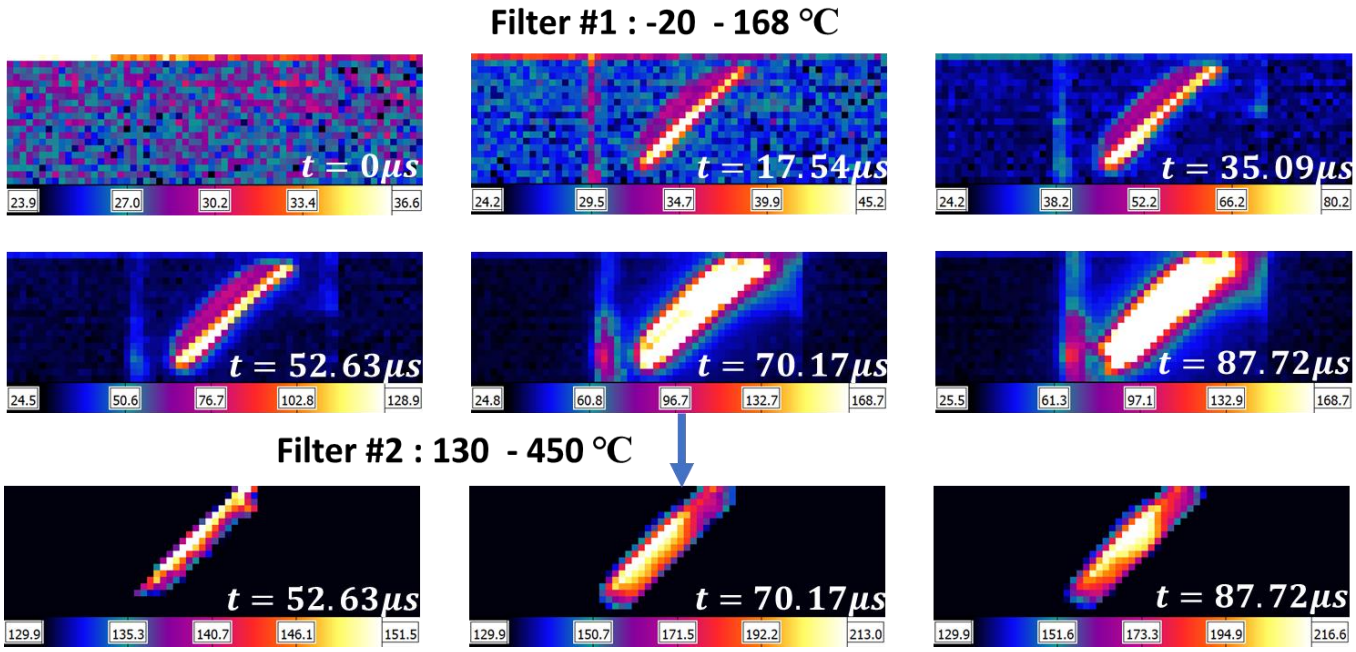

Figure 11: Snapshots of CP Ti at 57,000 FPS with 64x20 pixels resolution. The temperature rises along the gauge during the plastic deformation, including failure can be seen A large temperature increase caused by the shear plane is presented from $t = 70.17\ \mu s$ using both temperature range filters. This test presents the feasibility of measuring thin adiabatic shear planes.

Discussion

The main goal of this work is to compare the IR detector with the fast IR camera under dynamic loading and present some additional tests to elaborate upon the camera's capabilities. The comparative study was carried out on SS316L cylindrical specimens, while post failure analysis was done with Ti6Al4V cylindrical specimens, and the shear dominant behavior was tested using SCS made of CP Ti.

The comparative study on SS316L reveals an excellent correlation between the two techniques, detector, and camera. This correlation implies that the usually used TQC (β_{int}) can be deduced correctly using the camera since the extreme values and the general relation of the temperature and strain are preserved (at the measured points). However, due to the

lower frame rate of the camera as compared to the detector, some interpolation should be done between the measured points with the camera. For example, using linear interpolation between measured points can be done (unless a better correlation is known a -priori). This linear interpolation misses the local real slopes (as can be concluded from Figure 6) of the temperature rise as a function of the time (and also strain) and hence β_{diff} will be inaccurate, compared to the much more accurate slopes measured with the detector. This is true for most cases unless the relation between temperature and plastic strain (also time) is linear so that β_{diff} will be similar (as in the cases presented in this work to a good approximation), and in fact the case of linear relation yields $\beta_{diff} = \beta_{int}$. One should be alerted of this limitation (linear interpolation) when using e.g., unstable material going phase transition during deformation like SS304. In this case, the temperature may fluctuate a lot with time, breaking the linear relationship between temperature and strain [6]. These fluctuations may cause instantaneous increases or decreases in temperature which will affect the β_{diff}, and will probably be detected by the detector but not by the camera. Another issue that one should pay attention to is that measuring temperature rise for materials with low ductility akin to a short time to failure, will be much simpler (if not solely possible) with the detector due to its much higher sampling rate.

The failure along a shear plane test using Ti6Al4V has shown that post-failure behavior using SHPB experiments can be tested using the fast IR camera due to the full field measurement ability. The added value from such experiments might be great since there is a large temperature rise, e.g., a flammable gas might ignite if stored in a pressure vessel made of Ti6Al4V upon failure (strength considerations are another issue). This kind of analysis isn't possible using the detector since the detector measures a very localized area. This localized measurement, while measuring inhomogeneous and very local phenomena, implies that one may easily miss the shear plane using a detector. Moreover, at longer times, the incident bar intersects the detectors line of sight due to its movement which in turn interferes with the measured values.

When the shear plane is known or predefined as in the case of the SCS test with CP Ti, both the detector and camera might work. It is shown that although the camera's pixels are large, it is possible to follow the temperature rise in a very narrow shear plane.

Both experiments involving shear planes (and then fracture planes friction) had a large temperature rise which could be evaluated in one experiment using a detector while two experiments were needed for the camera. The IR detector was calibrated in these tests, for

each specific material, to the desired temperature range of up to about 350 °C. Unlike the detector, the camera has calibrated ranges of temperatures for each lens precluding a continuous measurement over a wide temperature range. Hence at least two tests had to be performed in this case of shear planes in Ti6Al4V and CP Ti, one for the first temperature range of -20 – 168 °C and the other for the next range of 129 – 450 °C.

Table 1 summarizes the as the outcomes of the present study as pros and cons of the IR detector and fast IR camera. It is important to emphasize that this comparative table is for the detector and camera used in this study. The table might be slightly different if for example other optics were used with the camera enabling better resolution by reducing the pixel size, or larger areas could be tested using an array of detectors instead of a single detector. However, the general picture will probably remain similar.

	Detector	**Camera**
Sampling rate	Very high – 1.5 MHz	High – 90 kHz
Calibration	Repeated and thorough calibration needed	No calibration needed
Ease of use	Complex, with many fixed parts	Versatile and flexible
Proven technique	Well known & proven	Relatively new and less tested
Measurement field	Narrow area of measurement	Full-field map
Resolution	Detector size 0.25X0.25 mm	Each pixel is 0.55X0.55 mm
Cooling system	Liquid nitrogen	Built-in cooler
Range of measurement	Continuous up to calibrated temperature	Discrete temperature range measurement
Low ductility materials	Partially applicable	Not applicable
$\boldsymbol{\beta_{int}}$ **evaluation**	Able to evaluate β_{int}	Able to evaluate β_{int}
$\boldsymbol{\beta_{diff}}$ **evaluation**	Able to evaluate β_{diff}	Limited to evaluate β_{diff}

Table 1: Pros and cons for the IR detector and high-speed IR camera as used in this study, for dynamic testing,.

Conclusions

A comparative study between the commonly used IR detectors (1.5 MHz) and the new technology of fast IR cameras (90 kHz) was done under large strain and strain rate to investigate

the temperature rise of metals. A satisfactory temperature correlation was achieved at the measured points, meaning that β_{int} (Taylor-Quinney coefficient) can be correctly computed using both techniques. However, the larger sampling rate of the detector enables it to reliably assess β_{diff} unlike the camera. The full field advantage of the camera was shown using a post failure analysis otherwise hard to achieve. In addition, a good ability to measure very local deformation using the camera was also presented. Although both techniques are sometimes interchangeable, as for β_{int} calculations, each of them has its advantages and hence should be chosen according to the necessity.

Funding Sources

This research did not receive any specific grant from funding agencies in the public, commercial, or not-for-profit sectors.

CRediT author statement

Gleb Gil Goviazin: Methodology, Formal analysis, Investigation, Writing - Original Draft, Visualization.

Amnon Shirizly: Conceptualization, Validation, Writing - Review & Editing, Visualization.

Daniel Rittel: Conceptualization, Methodology, Validation, Resources, Writing - Review & Editing, Visualization, Supervision.

Acknowledgments

Infrared Associates and Telops support with many processes and physical guidance are appreciated. Mr. I. Levin's assistance with specimens' supply and conducting the experiments is greatly appreciated.

Declaration

Conflicts of interest The authors declare that they have no conflict of interest.

References

1. Tresca MH (1878) On Further Applications of the Flow of Solids. Proceedings of the Institution of Mechanical Engineers 29:301–345. https://doi.org/10.1243/pime_proc_1878_029_017_02
2. Johnson GR, Cook WH (1985) Fracture characteristics of three metals subjected to various strains, strain rates, temperatures and pressures. Engineering Fracture Mechanics 21:31–48. https://doi.org/10.1016/0013-7944(85)90052-9
3. T BGI, Taylor GI, Quinney H (1934) The latent energy remaining in a metal after cold working. Proceedings of the Royal Society of London Series A, Containing Papers of a Mathematical and Physical Character 143:307–326. https://doi.org/10.1098/rspa.1934.0004
4. Rittel D (1999) On the conversion of plastic work to heat during high strain rate deformation of glassy polymers. Mechanics of Materials 31:131–139. https://doi.org/10.1016/S0167-6636(98)00063-5
5. Rittel D, Kidane AA, Alkhader M, et al (2012) On the dynamically stored energy of cold work in pure single crystal and polycrystalline copper. Acta Materialia 60:3719–3728. https://doi.org/10.1016/j.actamat.2012.03.029
6. Zaera R, Rodríguez-Martínez JA, Rittel D (2013) On the Taylor-Quinney coefficient in dynamically phase transforming materials. Application to 304 stainless steel. International Journal of Plasticity 40:185–201. https://doi.org/10.1016/j.ijplas.2012.08.003
7. Rittel D, Zhang LH, Osovski S (2017) The dependence of the Taylor–Quinney coefficient on the dynamic loading mode. Journal of the Mechanics and Physics of Solids 107:96–114. https://doi.org/10.1016/j.jmps.2017.06.016
8. Rittel D, Bhattacharyya A, Poon B, et al (2007) Thermomechanical characterization of pure polycrystalline tantalum. Materials Science and Engineering A 447:65–70. https://doi.org/10.1016/j.msea.2006.10.064
9. Ghosh D, Kingstedt OT, Ravichandran G (2017) Plastic Work to Heat Conversion During High-Strain Rate Deformation of Mg and Mg Alloy. Metallurgical and Materials Transactions A: Physical Metallurgy and Materials Science 48:14–19. https://doi.org/10.1007/s11661-016-3825-8

10. Marchand A, Duffy J (1988) An experimental study of the formation process of adiabatic shear bands in a structural steel. Journal of the Mechanics and Physics of Solids 36:251–283. https://doi.org/10.1016/0022-5096(88)90012-9
11. Hartley KA, Duffy J, Hawley RH (1987) Measurement of the temperature profile during shear band formation in steels deforming at high strain rates. Journal of the Mechanics and Physics of Solids 35:283–301. https://doi.org/10.1016/0022-5096(87)90009-3
12. Kolsky H (1953) Stress waves in solids. Clarendon Press, Oxford
13. Engineering M, Hopkinson B, Kolsky H, Kolsky H (2011) Dynamic material properties Strain measurements in a split Hopkinson bar. 5–7
14. Li Z, Zhao S, Ritchie RO, Meyers MA Mechanical properties of high-entropy alloys with emphasis on face-centered cubic alloys. Prog Mater Sci 102:296–345
15. Wu Y-Q, Huang F-L A microscopic model for predicting hot-spot ignition of granular energetic crystals in response to drop-weight impacts. Mechanics of materials 43:835–852
16. Astakhov VP, Outeiro J, Davim JP (2019) Importance of Temperature in Metal Cutting and Its Proper Measurement/Modeling, 1st ed. 20. Springer International Publishing :, Cham :
17. Kapoor R, Nemat-Nasser S (1998) Determination of temperature rise during high strain rate deformation. Mechanics of Materials 27:1–12. https://doi.org/10.1016/S0167-6636(97)00036-7
18. Rittel D (1998) Transient temperature measurement using embedded thermocouples. Experimental Mechanics 38:73–78. https://doi.org/10.1007/BF02321647
19. Regev A, Rittel D (2008) Simultaneous transient temperature sensing of impacted polymers using infrared detectors and thermocouples. Experimental Mechanics 48:675–682. https://doi.org/10.1007/s11340-007-9096-y
20. Rittel D (1998) Experimental investigation of transient thermoelastic effects in dynamic fracture. International Journal of Solids and Structures 35:2959–2973. https://doi.org/10.1016/S0020-7683(97)00352-1
21. Hodowany J, Ravichandran G, Rosakis AJ, Rosakis P (2000) Partition of plastic work into heat and stored energy in metals. Experimental Mechanics 40:113–123
22. Macdougall DAS, Harding J (1998) The measurement of specimen surface temperature in high-speed tension and torsion tests. International Journal of Impact Engineering 21:473–488. https://doi.org/10.1016/S0734-743X(98)00007-4

23. Soares GC, Vázquez-Fernández NI, Hokka M (2021) Thermomechanical Behavior of Steels in Tension Studied with Synchronized Full-Field Deformation and Temperature Measurements. Experimental Techniques 45:627–643. https://doi.org/10.1007/s40799-020-00436-y
24. Vazquez-Fernandez NI, Soares GC, Smith JL, et al (2019) Adiabatic Heating of Austenitic Stainless Steels at Different Strain Rates. Journal of Dynamic Behavior of Materials 5:221–229. https://doi.org/10.1007/s40870-019-00204-z
25. Seidt JD, Kuokkala VT, Smith JL, Gilat A (2017) Synchronous Full-Field Strain and Temperature Measurement in Tensile Tests at Low, Intermediate and High Strain Rates. Experimental Mechanics 57:219–229. https://doi.org/10.1007/s11340-016-0237-z
26. Soares GC, Hokka M (2022) Synchronized Full-Field Strain and Temperature Measurements
27. Yoshida S, Lamberti L, Sciammarella C (2016) Advancement of Optical Methods in Experimental Mechanics, Volume 3. Springer International Publishing
28. Rosakis P, Rosakis AJ, Ravichandran G, Hodowany J A thermodynamic internal variable model for the partition of plastic work into heat and stored energy in metals. J Mech Phys Solids 48:581–607
29. Zhouhua L, Lambros J (2001) Strain rate effects on the thermomechanical behavior of polymers. International Journal of Solids and Structures 38:3549–3562. https://doi.org/https://doi-org.ezlibrary.technion.ac.il/10.1016/S0020-7683(00)00223-7
30. Mason JJ, Rosakis AJ, Ravichandran G (1994) On the strain and strain rate dependence of the fraction of plastic work converted to heat: an experimental study using high speed infrared detectors and the Kolsky bar. Mechanics of Materials 17:135–145. https://doi.org/10.1016/0167-6636(94)90054-X
31. Zehnder AT, Rosakis AJ (1990) Experimental measurement of the temperature rise generated during dynamic crack growth in metals. Applied Mechanics Reviews 43:S260–S265. https://doi.org/10.1115/1.3120822
32. Zehnder AT, Rosakis AJ (1991) On the temperature distribution at the vicinity of dynamically propagating cracks in 4340 steel. Journal of the Mechanics and Physics of Solids 39:385–415. https://doi.org/10.1016/0022-5096(91)90019-K
33. Potdar YK, Zehnder AT (2004) Temperature and Deformation Measurements in Transient Metal Cutting. Experimental Mechanics 44:1–9. https://doi.org/10.1177/0014485104039623

34. Zehnder AT, Guduru PR, Rosakis AJ, Ravichandran G (2000) Million frames per second infrared imaging system. Review of Scientific Instruments 71:3762–3768. https://doi.org/10.1063/1.1310350
35. Guduru PR, Rosakis AJ, Ravichandran G (2001) Dynamic shear bands: An investigation using high speed optical and infrared diagnostics. Mechanics of Materials 33:371–402. https://doi.org/10.1016/S0167-6636(01)00051-5
36. Smith JL, Seidt JD, Gilat A, et al (2019) Full-Field Determination of the Taylor-Quinney Coefficient in Tension Tests of Ti-6Al-4V at Strain Rates up to 7000 s−1, 1st ed. 20. Springer International Publishing :, Cham :
37. Soares GC, Hokka M (2021) The Taylor–Quinney coefficients and strain hardening of commercially pure titanium, iron, copper, and tin in high rate compression. International Journal of Impact Engineering 156:. https://doi.org/10.1016/j.ijimpeng.2021.103940
38. Jia B, Rusinek A, Pesci R, et al Simple shear behavior and constitutive modeling of 304 stainless steel over a wide range of strain rates and temperatures. Int J Impact Eng 154:
39. Zubelewicz A (2019) Century-long Taylor-Quinney interpretation of plasticity-induced heating reexamined. Scientific Reports 9:1–7. https://doi.org/10.1038/s41598-019-45533-0
40. Boley BA (1997) Theory of thermal stresses / by Bruno a. Boley and Jerome H. weiner. Dover, Mineola
41. Annaratone Donatello (2010) Engineering Heat Transfer by Donatello Annaratone., 1st ed. 20. Springer Berlin Heidelberg, Berlin, Heidelberg
42. TELOPS (2020) High-Performance Infrared Cameras - TELOPS infrared cameras user’s guide, Revision 8. TELOPS
43. Nieto-Fuentes JC, Osovski S, Rittel D (2020) High-speed infrared thermal measurements of impacted metallic solids. MethodsX 7:100914. https://doi.org/10.1016/j.mex.2020.100914
44. Rabin Y, Rittel D (2000) Infrared temperature sensing of mechanically loaded specimens: Thermal analysis. Experimental Mechanics 40:197–202. https://doi.org/10.1007/BF02325046
45. Dorogoy A, Rittel D, Godinger A (2015) Modification of the Shear-Compression Specimen for Large Strain Testing. Experimental Mechanics 55:1627–1639. https://doi.org/10.1007/s11340-015-0057-6

46. Rittel D, Lee S, Ravichandran G (2002) A shear compression specimen for large strain testing. Experimental Mechanics 42:58–64. https://doi.org/10.1007/BF02411052